Summary: An amphiphilic poly(*N*-propargylamide) with galactose and lauryloyl groups was synthesized by copolymerization of the corresponding *N*-propargylamide monomers using a Rh catalyst. The obtained copolymer formed a one-handed helical conformation and molecular aggregates in water. The observations by fluorescence microscopy in a cell culture experiment in the presence of dye-labeled copolymer indicated that the copolymer was incorporated into the cells.

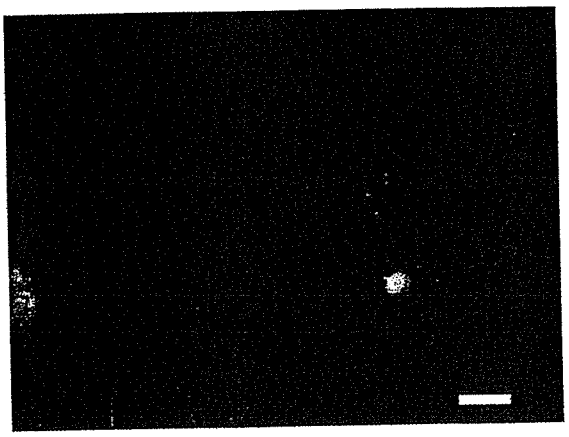

Localization of rhodamine B-labeled copolymer **8** in human aortic endothelial cells (fluorescence image).

Amphiphilic Poly(*N*-propargylamide) with Galactose and Lauryloyl Groups: Synthesis and Properties

Masakazu Suenaga,[1] *Yoshiro Kaneko,*[1] *Jun-ichi Kadokawa,**[1] *Takehiro Nishikawa,*[2] *Hidezo Mori,*[2] *Masayoshi Tabata*[3]

[1]Department of Nanostructured and Advanced Materials, Graduate School of Science and Engineering, Kagoshima 890-0065, Japan
Fax: +81-99-285-3253; E-mail: kadokawa@eng.kagoshima-u.ac.jp
[2]National Cardiovascular Center, Suita, Osaka 565-8565, Japan
[3]Department of Molecular Chemistry, Graduate School of Engineering, Hokkaido University, Sapporo 060-8628, Japan

Received: July 19, 2006; Accepted: October 10, 2006; DOI: 10.1002/mabi.200600228

Keywords: amphiphiles; conjugated polymers; copolymerization; dynamic light scattering; nanoparticles; polyacetylenes

Introduction

Synthesis of polymers having sugar residues, so-called glycopolymers, has been widely investigated to seek biological applications because of their versatile functions.[1,2] It has been demonstrated that these glycopolymers can bind specifically to carbohydrate-recognition proteins, toxins, viruses, and cells, and, thus, these polymers can be utilized as cell culture substrates with specific cell recognition sites, as well as in targeting drug delivery systems.[1,2] The clustered saccharide ligands conjugated to the polymeric main chains are involved in these specific recognition processes. Most of the previously prepared glycopolymers have been based on a flexible polymer backbone, such as polystyrene and polyacrylamide.[3,4] This flexible nature of the glycopolymers causes the disordered orientation of the sugar residues in the glycopolymers. Regular orientation of the sugar residues is necessary for efficient interaction between the glycopolymers and receptor molecules. In this sense, the spatially regulated orientation of the sugar residues should be realized by attaching the sugar residues to a polymer backbone with a rigid conformation. The sugar residues attached to the rigid polymer backbone may give rise to the ordered orientation that can improve the molecular recognition of sugar residues by specific cell receptors. This is because the spatial regulation of the sugar residues is significant in molecular recognition as well as the chemical structure of the sugar molecules.[5]

From the above viewpoints, rigid glycopolymers with π-conjugated polymer backbones would be a novel type of bio-inspired polymers, which could exhibit multiple valence states and interact specifically and firmly with targets such as cell surface receptors and biomacromolecules. In some previous works, rigid glycopolymers having various π-conjugated main chains, such as polythiophene,[6] poly(*p*-phenylene ethynylene),[7] polyisocyanide,[8] polyaniline,[9] poly(*p*-phenylene vinylene),[10] and poly(phenylacetylene), have already been synthesized.[11] In the series of these studies, we reported the synthesis of poly(*N*-propargylamide) (**2**) with sugar residues. It contained a *cis*-polyacetylene main chain and was obtained by the rhodium-catalyzed polymerization of a *N*-propargylamide monomer (**1**) that had a galactose residue (Scheme 1).[12] Since polymerizations of the *N*-propargylamide monomers having various substituted groups using Rh catalyst have been widely reported to produce the corresponding poly(*N*-propargylamide) derivatives with *cis*-isomers,[13] we also investigated the copolymerization of **1** with *N*-propargylamide derivative **3** having a hexanoyl group to produce the amphiphilic glycopolymer **4**, as shown in Scheme 1. We tested the solubility of copolymer **4** in various solvents to confirm whether the copolymer exhibits an amphiphilic property. Although the homopolymer **2** is insoluble in common organic solvents, the copolymer **4** can be dissolved in some polar organic solvents, such as dimethyl sulfoxide (DMSO) and *N,N*-dimethylformamide (DMF), as well as in aqueous medium. However, the copolymer still exhibits a hydrophilic nature rather than an amphiphilic nature. We assumed that insufficient amphiphilicity of copolymer **4** could be attributed to poor hydrophobic property of the hydrophobic part.

In this study, we chose a more hydrophobic monomer: *N*-propargylamide monomer **5** having a longer alkyl chain, i.e., the lauryloyl group, as the hydrophobic part of the amphiphilic copolymer. The monomer **5** was copolymerized with **1** in the presence of Rh catalyst to give the corresponding amphiphilic copolymer **6** (Scheme 2). The resulting copolymer **6** can be expected to have the ability to conduct molecular aggregation in water, which is driven by intermolecular and intramolecular association of the hydrophobic lauryloyl groups.

We believe that such molecular aggregates of the amphiphilic copolymer should play a significant role in the field of targeted drug delivery. The idea is supported by the following characteristics of the molecular aggregates:

1) Drug carriers with nanometer dimensions can be obtained by molecular aggregation of amphiphilic copolymers.
2) Nano-sized aggregates can remain in the bloodstream for an extended period because of the size-dependent uptake in the reticuloendothelial system.
3) Drug molecules with hydrophobic natures can be loaded into hydrophobic milieus formed by the association of hydrophobic long alkyl chains; otherwise the drug molecules could be directly attached to the constituent monomer molecules of the copolymer.
4) Sugar residues of the copolymer can function as recognition sites for target cells and tissues as well as providing the hydrophilic character of the amphiphilic copolymer.

Therefore, we studied the *in vitro* cell uptake of the molecular aggregates of the amphiphilic copolymer. For this purpose, the fluorescent marker, rhodamine B, was introduced into the amphiphilic copolymer. In this article, we report the synthesis of the amphiphilic

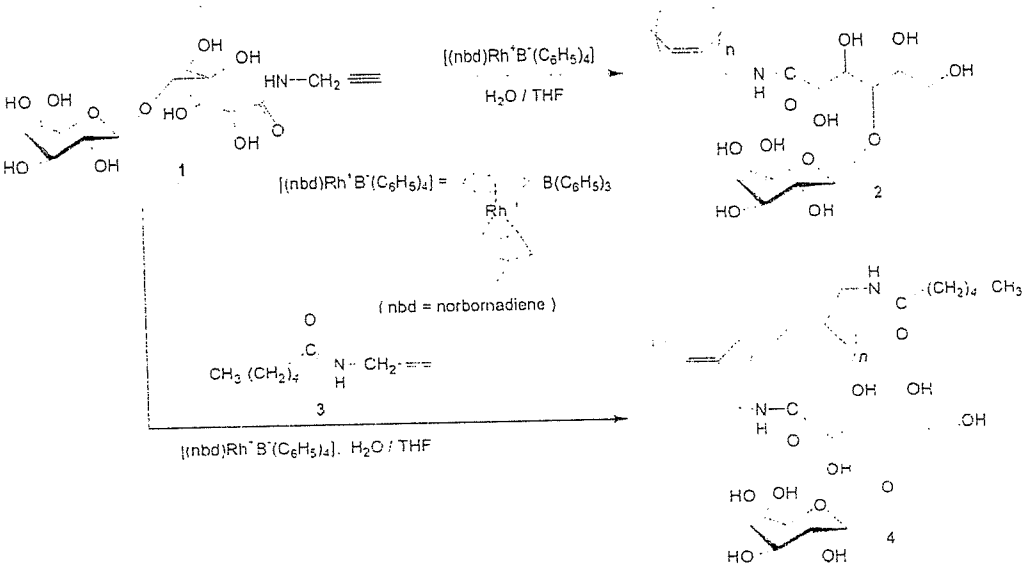

Scheme 1. Polymerization of **1** and copolymerization of **1** with **3**.

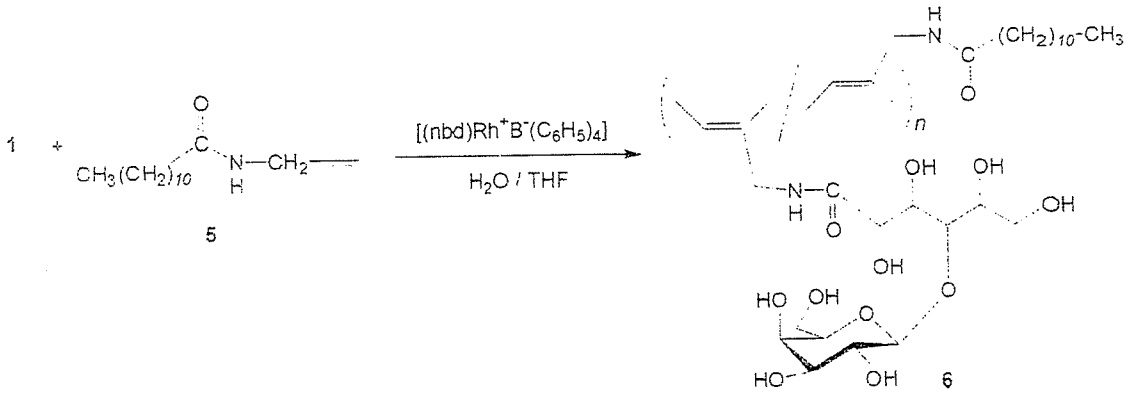

Scheme 2. Copolymerization of 1 with 5.

poly(*N*-propargylamide) **6** by Rh-catalyzed copolymerization, evaluation of its molecular aggregation in water [gel permeation chromatography (GPC) characterization, scanning electron microscopy (SEM) observation, and dynamic light scattering (DLS) measurement] and secondary conformation [circular dichroism (CD) spectra], and cell uptake of the nanoaggregate of the rhodamine-labeled amphiphilic copolymer (fluorescence microscopy).

Experimental Part

Materials

Monomer **1** and catalyst (nbd)Rh$^+$B$^-$ $(C_6H_5)_4$ were prepared according to the literature.[12,13] Tetrahydrofuran (THF) used as polymerization solvent was purified by distillation. Other reagents and solvents were used as received without further purification.

Synthesis of Monomer 5

Monomer **5** was synthesized by a method similar to that used for **3**.[15] Under argon, *N*-propargylamine hydrochloride (0.915 g, 10.0 mmol) was dissolved by slight warming in anhydrous acetonitrile (12.0 mL), and triethylamine (3.35 mL, 24.0 mmol) was added to the solution at room temperature. Then a solution of lauryloyl chloride (2.36 mL, 10.0 mmol) in anhydrous acetonitrile (12.0 mL) was added dropwise to the solution. After the mixture was stirred for 2 h, the reaction solution was concentrated by evaporation. The residue was dissolved in ethyl acetate and the solution was washed successively three times with 2 mol·L^{-1} hydrochloric acid and with saturated $NaHCO_3$ aqueous solution. The organic layer was dried over anhydrous Na_2SO_4, filtered, and evaporated. The residue was subjected to column chromatography on silica gel (hexane:ethyl acetate = 4:1, v/v) to isolate **5** (1.38 g, 5.82 mmol) in 58.2% yield.

^{1}H NMR ($CDCl_3$): δ = 0.88 (t, J = 7.2 Hz, CH_3, 3H), 1.28 [m, $CH_3(CH_2)_8$, 16H], 1.62 (m, CH_2CH_2C=O, 2H), 2.19 (t, J = 7.8 Hz, CH_2C=O, 2H), 2.23 (t, J = 2.4 Hz, H–C≡C, 1H), 4.05–4.06 (m, CH_2N, 2H), 5.57 (s, NH, 1H).

Synthesis of Monomer 7

Under argon, triethylamine (0.836 mL, 6.00 mmol) was added to a solution of *N*-propargylamine hydrochloride (0.549 g, 6.00 mmol) and rhodamine B (1.92 g, 4.0 mmol) in anhydrous methanol (10.0 mL) at 0 °C. To the solution was added 1-[(3-dimethylamino)propyl]-3-ethylcarbodiimide hydrochloride (1.15 g, 6.00 mmol) as a condensing agent at 0 °C and the mixture was stirred for 17 h at room temperature. The precipitated material was isolated by filtration and dried under the reduced pressure to give **7** (0.472 g, 0.915 mmol) in 23.0% yield.

^{1}H NMR ($CDCl_3$): δ = 1.16 (m, CH_3, 12H), 1.77 (t, J = 2.4 Hz, H–C≡C, 1H), 3.33 (m, NCH_2CH_3, 8H), 3.95 (d, J = 1.8 Hz, CH_2C≡, 2H), 6.26–7.93 (m, aromatics, 10H).

Copolymerization of 1 with 5

A typical copolymerization procedure was as follows (entry 1, Table 1). Under argon, a solution of **5** (0.0356 g, 0.150 mmol) in THF (0.90 mL) and a solution of catalyst (0.00630 g, 0.0125 mmol) in THF (0.90 mL) were added to a solution of **1** (0.0397 g, 0.100 mmol) in water (0.20 mL) in this order at 30 °C. After the mixture was stirred at 30 °C for 140 min, the reaction mixture was concentrated by evaporation and dried under reduced pressure. The residue was dissolved in a small amount of DMSO and the solution was poured into a large amount of methanol to precipitate the polymeric product. The precipitate was isolated by filtration and was dried under reduced pressure to give **6** (0.0588 g) in 78.1% yield.

^{1}H NMR (DMSO-d_6): δ = 0.84 (CH_3), 1.21 [$CH_3(CH_2)_8$], 1.45 (CH_2CH_2C=O), 2.15 (CH_2C=O), 3.0–3.9 {–CH(O–D-gal)–CH(OH)–CH_2OH, =CCH_2–, H2–H6 of D-gal}, 4.04 [C(=O)CH(OH)CH(OH)–], 4.29 {C(=O)CH(OH)– and H1(β) of D-gal}, 4.55, 4.79, 5.22 (OH), 6.11 (–CH=C–), 7.93 (NH).

Copolymerization of 1, 5, and 7

Under argon, a solution of **5** (0.0285 g, 0.120 mmol) and **7** (0.0929 g, 0.180 mmol) in THF (0.90 mL) and a solution of catalyst (0.0166 g, 0.0330 mmol) in THF (0.90 mL) were

Table 1. Results for copolymerization of 1 with 5 with Rh catalyst in THF–water (9:1) solvent.

Entry	Feed ratio[a]	Time	Yield[b]	Unit ratio[c]	$\bar{M}_n$[d]	$\bar{M}_w/\bar{M}_n$[d]	$[\alpha]_D$[e]
	1:5	min	%	1:5			degrees
1	1.0:1.5	140	78.1	1.0:0.92	9 100	1.30	
2	1.0:1.0	195	62.5	1.0:0.88	6 200	1.63	
3	1.0:0.67	240	57.0	1.0:0.35	5 200	1.60	96.8
4	1.0:0.50	260	68.9	1.0:0.32	9 600	1.64	142.3
5	1.0:0.33	200	69.9	1.0:0.26	7 100	1.50	173.6
6	1.0:0.20	210	78.1	1.0:0.17	9 700	1.30	185.6

[a] [Catalyst]/[1 + 5] = 0.05, reaction temperature: 30 °C.
[b] Fraction insoluble in methanol.
[c] Determined from ^{1}H NMR spectra.
[d] Determined by GPC with water as eluent using pullulan standards, sample concentration = 0.1 mg · mL^{-1}.
[e] Measured by polarimetry in water, c = 1.0 g · dL^{-1} at 20 °C.

added to a solution of 1 (0.143 g, 0.360 mmol) in water (0.20 mL) in this order at 30 °C. After the mixture was stirred at 30 °C for 18 h, the reaction mixture was concentrated by evaporation and dried under reduced pressure. The residue was dissolved in a small amount of DMSO and the solution was poured into a large amount of methanol to precipitate the polymeric product. The precipitate was isolated by filtration and dried under reduced pressure to give **8** (0.164 g) in 62.0% yield.

^{1}H NMR (DMSO-d_6 + D_2O): δ = 0.93 ($CH_3CH_2CH_2$), 1.16 (CH_3CH_2N), 1.25 [$CH_3(CH_2)_8$], 1.50 ($CH_2CH_2C{=}O$), 3.0–4.5 (sugar protons and =C–CH_2–), 6.16 (HC=), 7.0–8.0 (aromatics).

Cell Culture Experiment

Human aortic endothelial cells (HAECs) were purchased as cryopreserved samples of third passage (Lot: 3F1346) from Cambrex (Wakersville, MD, USA). The HAECs were subcultured once and stored in liquid nitrogen until cell culture experiment. The HAECs used in the experiment were fourth passage. Each well of a 12-well plate of polystyrene (Iwaki) was filled with 1 mL of a supplemented culture medium (EGM-2; Lot: 08103123, Cambrex) and equilibrated at 37 °C in a humidified incubator under 5% CO_2 for 30 min before cell seeding. After the frozen cells were thawed at 37 °C, 10 μL of the cell suspension was seeded in each well. The initial cell density was 2.2×10^5 cells · cm^{-2}. Cell viability assessed by the trypan blue exclusion test was 83% for the cell suspension. The cell seeded plates were placed in a humidified incubator at 37 °C under 5% CO_2. The HAECs were cultured for 48 h. Cell culture mediums were replaced with fresh medium 24 h after cell seeding. At 48 h after cell seeding, cell culture mediums were each replaced with an aqueous suspension of copolymer **8**. Then the HAECs were cultured in the polymer suspension for 1, 6, and 24 h in a humidified incubator at 37 °C under 5% CO_2 to study cellular uptake of nanoaggregates of copolymer **8**. For fluorescence microscopy observation, the cells were fixed by immersion in 10% formaldehyde neutral buffer solution (Nacalai Tesque) at room temperature (22 °C) for 15 min and were washed three times with phosphate-buffered saline (PBS; Gibco). Fluorescence images of the cells were taken with a fluorescence microscope (IX71; Olympus) equipped with a CCD camera (DP70; Olympus). Fluorescence intensity of the incorporated copolymer **8** was measured by integrating the fluorescence intensity observed at each pixel of the fluorescence images using image analysis software (Fluoview ver. 5.0; Olympus).

Measurements

NMR spectra were recorded on a JEOL EC'A 600 spectrometer. Optical rotations were measured with a Jasco P-1030 digital polarimeter. GPC analyses were performed by using a TOSOH 8012 with refractive index detection under the following conditions: Shodex Asahipak GF-310HQ column with water as eluent at a flow rate of 0.5 mL · min^{-1}. The calibration curve was obtained using pullulan standards. CD and UV-vis spectra were measured in a quartz cell (thickness 1 cm) at room temperature using a Jasco J-820 spectropolarimeter and Shimadzu UV160A spectrophotometer, respectively. The SEM images were obtained using a Hitachi S-4100 electron microscope. The DLS measurement was performed on a Zetasizer 3000 (Malvern Instruments). Fluorescence spectra were obtained on a fluorescence spectrometer (Shimadzu) using a quartz cuvette (1-mm path length).

Results and Discussion

Copolymerization of 1 with 5

The polymerization of monosubstituted acetylene derivatives has been widely investigated using Rh complex catalysts, which enables stereoselective synthesis of the corresponding polyacetylenes of the *cis*-isomers.[16] As

already reported in our previous publication, **1** was polymerized using (nbd)Rh$^+$B$^-$(C_6H_5)$_4$ as the catalyst at around 25 °C to 50 °C in a mixed solvent of THF and water (9:1, v/v).[12] In this study, we performed the copolymerization of **1** with **5** under similar conditions. The copolymerization with various feed ratios of **1** to **5** was carried out using the Rh catalyst (5.0 mol-% for **1** + **5**) at 30 °C in a THF-water mixed solvent under argon. After polymerization, the resulting mixture was concentrated and then dissolved in DMSO. The solution was poured into a large amount of methanol to precipitate the polymeric product. The precipitate was isolated by filtration and dried under reduced pressure to give the copolymer **6** (Table 1). The copolymer was soluble in water and DMSO, and its $\overline{M}_n$ value was estimated by GPC analysis with water as eluent using pullulan standards. Figure 1a shows the ^{1}H NMR spectrum of the copolymer (entry 1, Table 1) measured in DMSO-d_6. The signals due to the sugar and alkyl protons are observed at around δ 3.0–4.3 (signals **e**–**h**) and δ 0.84, 1.21, 1.45, 2.15 (signals **a**–**d**), respectively. In addition to these signals, signal **i** ascribed to the main-chain proton of –CH=C– appears centered at δ 6.11. The chemical shift of this signal realistically corresponds to the *cis*-isomer. Furthermore, there is no signal due to the *trans*-isomer at lower magnetic field from the *cis*-signal. The NMR results support structure **6** as that of the copolymer, which is mainly composed of *cis*-isomer. The unit ratio of the copolymer is calculated by the integrated ratio of signal **a** and signal **i**.

Table 1 shows the copolymerization results obtained by the various feed ratios of **1** to **5**. The yields and the $\overline{M}_n$ values are 57.0–78.1% and 5 200–9 700, respectively. The unit ratios of **5** in the copolymers increase with increasing molar ratios of **5** in the feeds. In all cases, however, the ratios of **5** in the copolymers are lower than those in the feeds. This is probably because the copolymers with higher

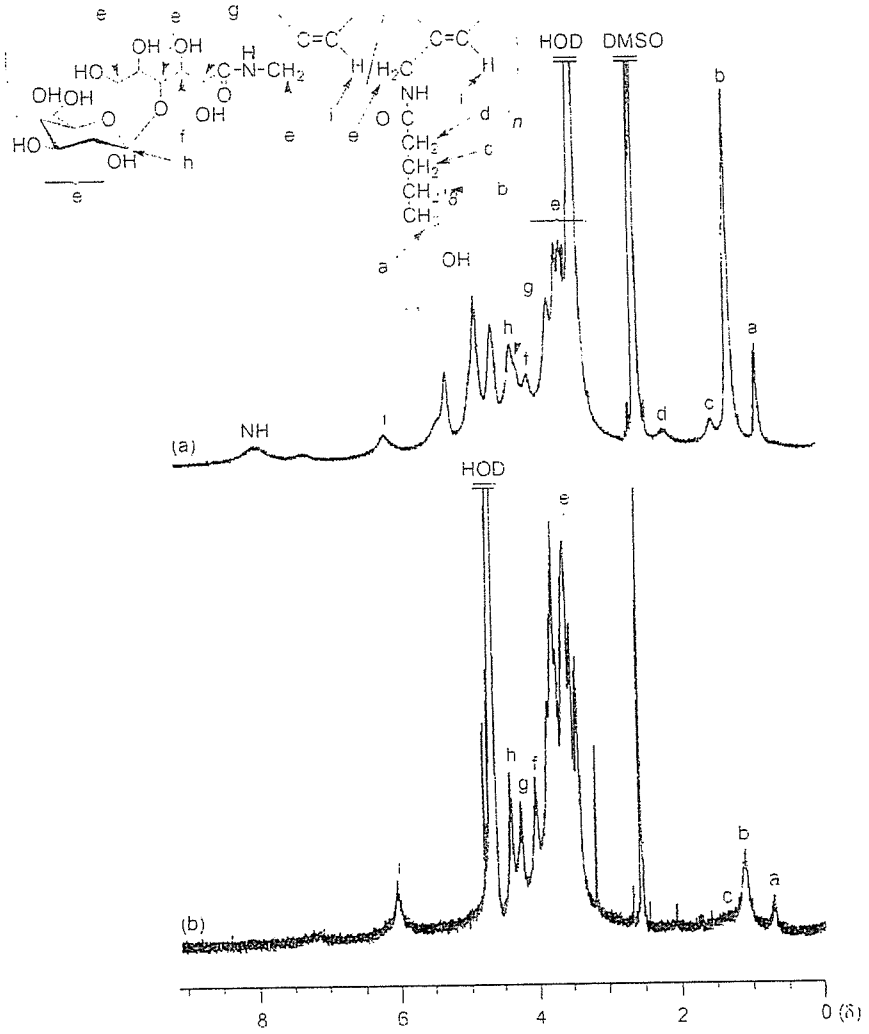

Figure 1. ^{1}H NMR spectra of copolymer **6** (entry 1, Table 1) in DMSO-d_6 (a) and D_2O (b).

contents of the unit **5** are lost as methanol-soluble fractions during the isolation procedure. The optical rotations of the copolymers with the higher contents of the sugar units were larger than those with the lower contents.

Formation of Molecular Aggregates in Water

When the copolymerization was followed by thin-layer chromatography (TLC) on silica gel (methanol: chloroform = 2:1 for **1**; hexane: ethyl acetate = 1:1 for **5**), **1** appeared to be consumed at the early stage of the reaction; subsequently, the consumption of **3** at a later stage was confirmed. This indicated that **6** had the block copolymeric sequence between the unit **1** and the unit **5** rather than in random style. In fact, the intensities of the alkyl signals **a–d** in the ^{1}H NMR spectrum of **6** in D_2O (Figure 1b) are obviously lower than those of the same copolymer measured in DMSO-d_6 (Figure 1a). The NMR results suggest formation of micelle-like aggregates having the outer hydrophilic sugar residues and the inner hydrophobic lauryloyl groups in water, and this was attributed to the block copolymeric sequence. The formation of molecular aggregates of **6** in water was also confirmed by the GPC measurements on aqueous solutions of **6** (entry 5, Table 1, the unit ratio of **1** to **5** = 1.0:0.26) ranging in concentration from 0.05 to 9.0 mg · mL^{-1}. Figure 2 shows the relations of the $\overline{M}_n$ values to the sample concentrations in the GPC experiments. The $\overline{M}_n$ values increase from ca. 6300 to ca. 11000 for concentrations higher than 0.70 mg · mL^{-1}. These data suggest the formation of molecular aggregates for the higher concentrations of **6** in water. The molecular aggregates of **6** were directly observed by SEM. The SEM image of the spin-coated sample from the aqueous solution of **6** (entry 4, Table 1, the unit ratio of **1** to **5** = 1.0:0.32) on aluminium plate (Figure 3) shows the particle-type molecular aggregates with average diameters of 20–40 nm. The particle sizes were also confirmed by DLS measurement. The mean particle diameter of the sample shown as entry 4 in Table 1 was 85.2 ± 14.1 nm. The difference in the aggregate sizes obtained by SEM and DLS can be attributed to the difference in the sample condition: dry for SEM and wet for DLS.

Secondary Conformation of 6

We already reported in our previous report that the CD spectrum of the homopolymer **2** in water showed the positive Cotton effect at 330 nm corresponding to the main-chain UV-vis absorption.[11,12] This indicated the possibility for formation of a one-handed helical conformation in the main chain of **2**. In this study, the CD analysis was also performed to reveal the secondary conformation of copolymer **6**. Figure 4 shows the CD spectra of **6** (entry 5, Table 1, unit ratio of **1** to **5** = 1.0:0.26) in comparison with those of copolymer **4** (unit ratio of **1** to **3** = 1.0:0.39) measured in DMSO and water at room temperature. The CD spectrum of **6** in DMSO (Figure 4a) shows the positive Cotton effect at 360 nm, corresponding to the main-chain UV-vis absorption. The positive Cotton effect also appeared at this region in the CD spectrum in water (Figure 4b), although its intensity was lower than that in DMSO. It has been reported that the helical structure of poly(*N*-propargylamides) is stabilized by the intramolecular hydrogen bonds between the pendant amide groups.[11] In polar solvents such as DMSO and water, therefore, the hydrogen bonds are readily broken to effect destabilization of the helical structure. The helical conformation of **6** in polar solvents is probably stabilized by the bulky substituents in the side chains of sugar and lauryloyl groups. These bulky groups shield the hydrogen bonds from the solvents, which consequently stabilizes the helical structure. This reasoning is also supported by comparison of the CD spectra of copolymer **4** (gray lines in

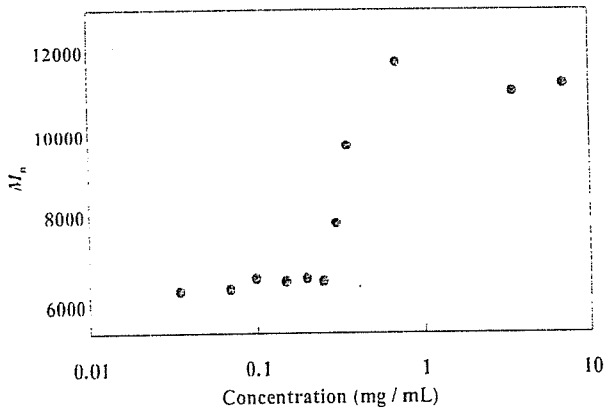

Figure 2. $\overline{M}_n$ values versus sample concentrations in GPC measurements with water as eluent (entry 5, Table 1).

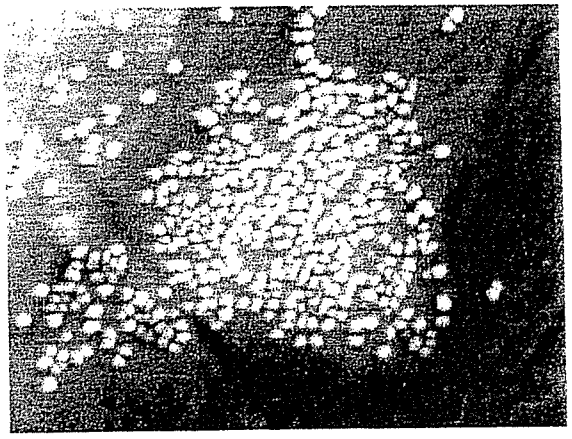

Figure 3. SEM image of **6**: the sample was prepared by spin coating of the dispersed solution of **6** (entry 4, Table 1) in water.

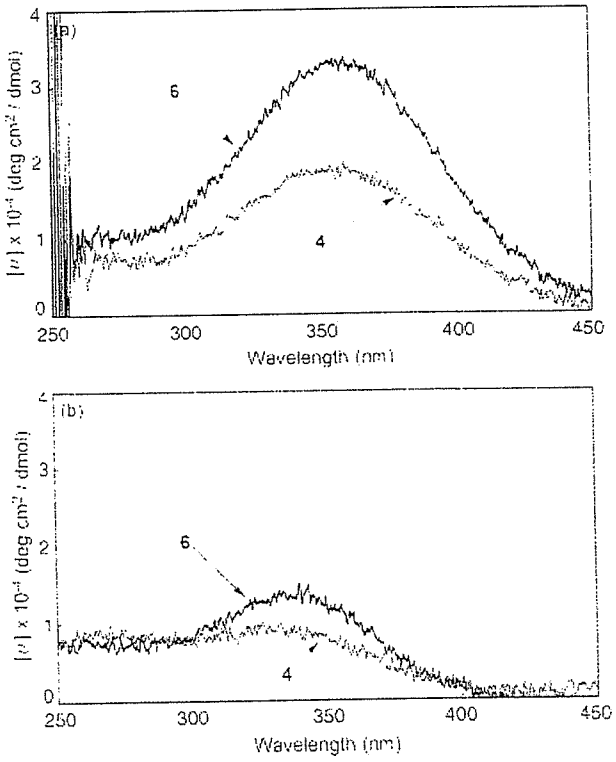

Figure 4. CD spectra of **6** (entry 5, Table 1, unit ratio: 1:5 : 1.0:0.26) and **4** (unit ratio: 1:3 : 1.0:0.39) in DMSO (a) and water (b) (c = 0.2 mmol·L^{-1}).

Figure 4a, b), which has the less bulky hexanoyl groups. The CD spectra of **4** show weaker Cotton effects than those of **6**, indicating the stabilization of the helical conformation as a result of the bulkiness of the pendant groups.

Cellular Uptake of Amphiphilic Copolymer 8

To evaluate cell uptake of the copolymer by fluorescence microscopy, the rhodamine B dye moiety was introduced into the amphiphilic copolymer. First, an *N*-propargylamide derivative **7** having a pendant rhodamine B moiety was prepared by condensation of *N*-propargylamine hydrochloride with rhodamine B in the presence of a condensing agent (1-[(3-dimethylamino)propyl]-3-ethylcarbodiimide hydrochloride) in methanol. Then, the isolated **7** was copolymerized with **1** and **5** under conditions similar to those described above (Scheme 3). Although **7** did not have homopolymerizability by Rh catalyst, the unit from **7** was slightly incorporated into the resulting terpolymer by the copolymerization. The existence of the rhodamine B moiety in the obtained terpolymer **8** was confirmed by appearance of the signals due to methyl protons of N-CH_2CH_3 as well as the aromatic protons in the ^{1}H NMR spectrum of the product. However, the intensities of the signals were too weak to determine the exact content of the dye moiety in the copolymer by the integration ratio. For comparison, hydrophilic copolymer **9** was synthesized by copolymerization of monomer **1** with monomer **7** using Rh catalyst (Figure 5).

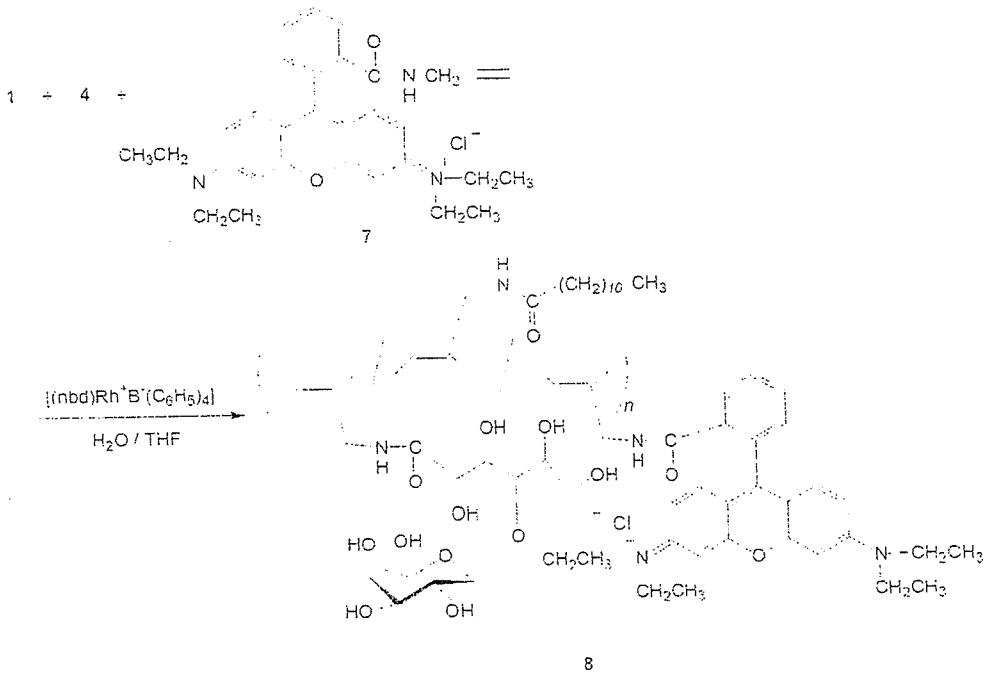

Scheme 3. Terpolymerization of **1**, **5**, and **7**.

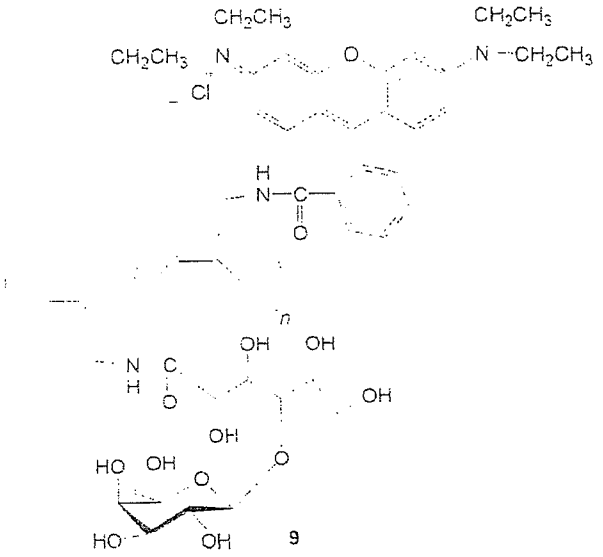

Figure 5. Structure of copolymer 9.

The cell uptake of terpolymer 8 was studied by culturing human aortic endothelial cells (HAECs) in a culture medium containing the terpolymer 8. Ten milligrams of 8 was suspended in 10 mL of culture medium EGM-2 and stirred for 3 h at room temperature. The suspension of 8 was sonicated at 25 W and 40 kHz for 5 min in an ultrasonic bath. The sonication was repeated twice. The obtained suspension was filtered through membrane filters with the pore sizes of 0.45 μm and 0.2 μm for sterilization. An aqueous solution of polymer 9 was prepared by following the above procedure. To evaluate the concentration of 8, a calibration curve (data not shown) was obtained by using the aqueous solution of 9 (1 mg · mL^{-1}) as a standard polymer sample to relate concentration to fluorescence intensity. The concentration of 8 was estimated to be 0.09 mg · mL^{-1} by using the calibration curve. The DLS measurement revealed that the polymer aggregates (nanoparticles) of 8 have a mean diameter of 114.9 ± 32 nm in a culture medium containing 10% bovine serum. HAECs were exposed to the polymer aggregates of 8 while they were cultured in the culture medium containing the amphiphilic polymer 8. After the prescribed period of culture, 1, 6, or 24 h, the HAECs were fixed in 10% formaldehyde neutral buffer solution for microscope observation. Figure 6 shows phase contrast (a), fluorescence (b), and merged (phase contrast – fluorescence) (c) images of HAECs after 24 h of incubation. The merged image demonstrates that red fluorescent light of rhodamine B was emitted from the sites where HAECs were located. This indicates that the polymer aggregates of 8 were incorporated into HAECs. The fluorescence images at each time of incubation are shown in Figure 7. The fluorescence images get brighter with the incubation time. To quantitatively evaluate cell uptake of nanoaggregates, fluorescence intensity per image (1 360 × 1 024 pixels) was determined by integrating the brightness at each pixel of the fluorescence image using image analysis software. The

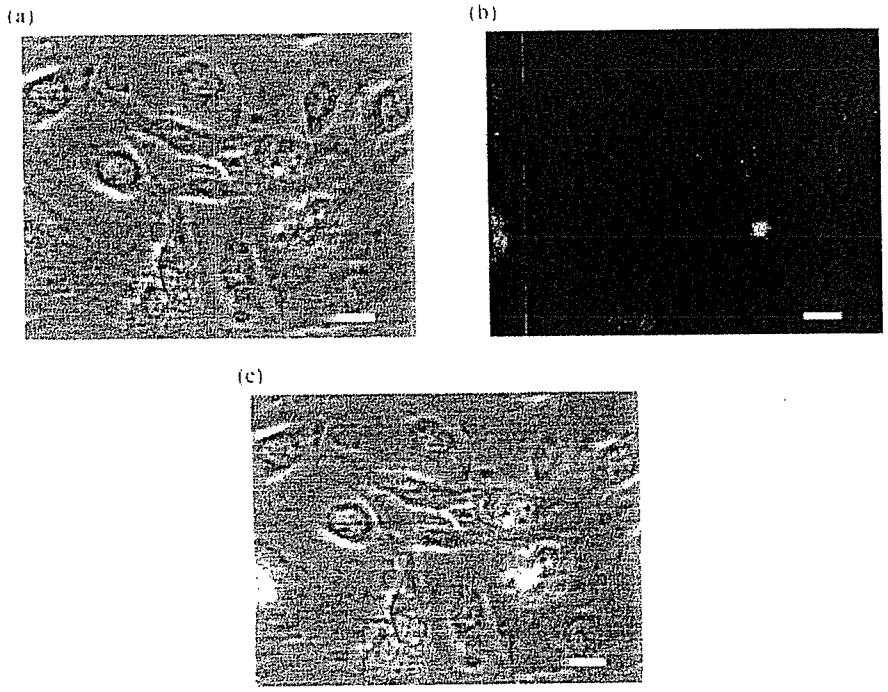

Figure 6a–c. Localization of rhodamine B-labeled copolymer 8 in human aortic endothelial cells. Phase contrast image (a), fluorescence image (b), and merged image of (a) and (b). Bars: 20 μm.

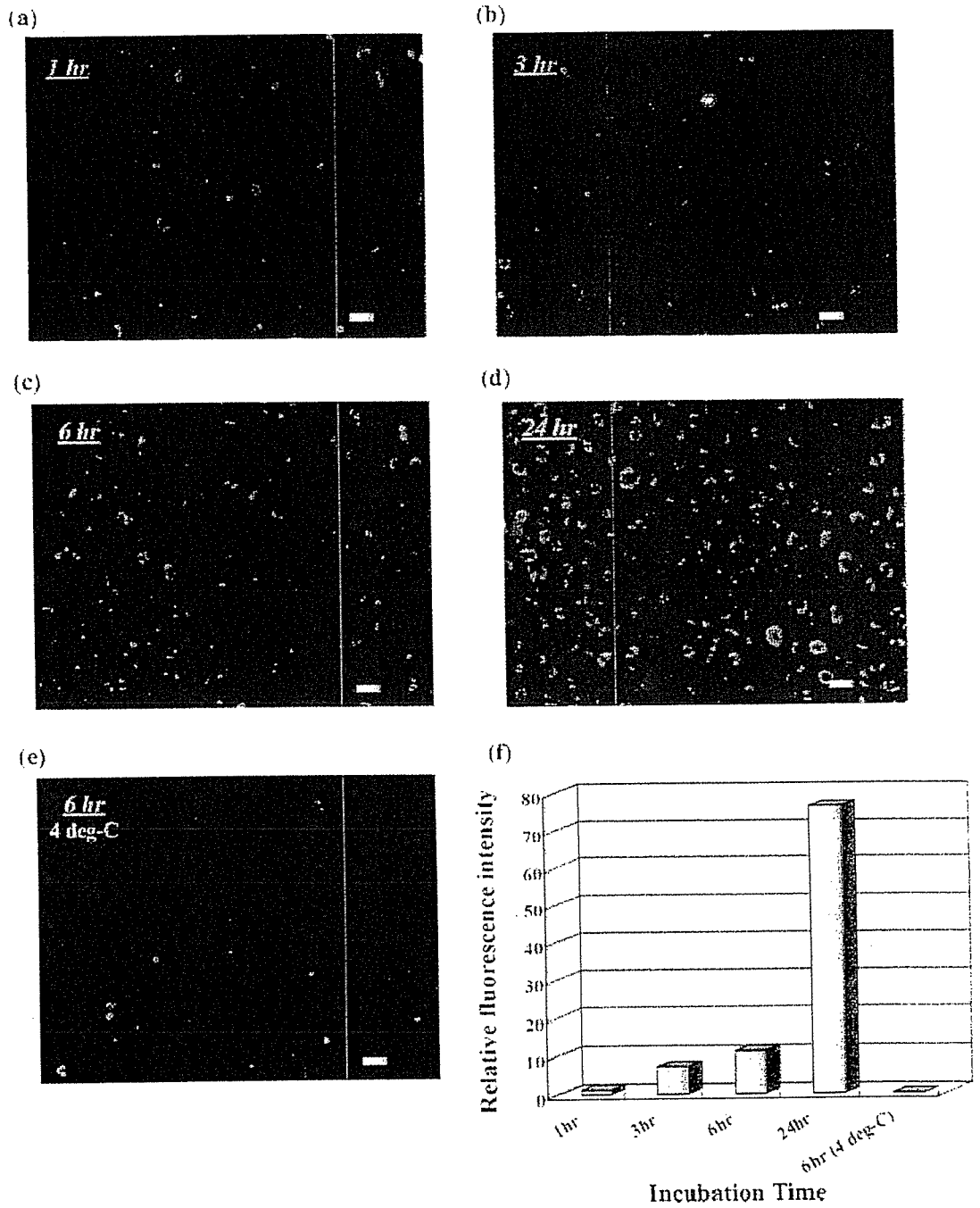

Figure 7a–f. Uptake of rhodamine B-labeled copolymer **8** by human aortic endothelial cells: incubation time, 1 h (a), 3 h (b), 6 h (c), 24 h (d) (incubation at 37 °C), and 6 h (incubation at 4 °C) (e). Bars: 20 μm. The uptake is quantitatively represented as relative fluorescence intensity in the bar graph (f).

fluorescence intensity was normalized in a ratio of the fluorescence intensity at each incubation time to that at 1 h of incubation. The ratio was termed as the relative fluorescence intensity. The time course of the relative fluorescence intensity is shown in Figure 7f and indicates that HAECs incorporated progressively more nanoaggregates of **8** during the incubation time. The relative fluorescence intensity was 7-fold at 3 h, 11-fold at 6 h, and 76-fold at 24 h of incubation. In contrast, the relative fluorescence intensity dropped considerably and was only 12% of the control level (1 h at 37 °C) when HAECs were exposed to the nanoaggregates of **8** at 4 °C for 6 h. The fact that the temperature triggered a dramatic decrease in the relative fluorescence intensity suggests that the nanoag-

gregates are incorporated into HAECs by endocytosis. Endocytosis is known as a cellular process that is coupled with temperature-dependent metabolic activities.[18] Furthermore, it is known that some receptors and membrane microdomains of endothelial cell are involved in endocytosis.[19] However, it is not clear which of the endocytic pathways is responsible for the uptake of the nanoaggregates. This issue is now under investigation.

Conclusion

In this study, we investigated synthesis of the amphiphilic poly(*N*-propargylamide) **6** containing both sugar residues (hydrophilic part) and long alkyl chains (hydrophobic part) in order to develop a novel nanoaggregate based on the self-organization of amphiphilic polymers with rigid backbone. The desired polymer was prepared by copolymerization of the two *N*-propargylamide monomers **1** and **5** having a galactose residue and a lauryloyl group, respectively, catalyzed by a Rh complex. The GPC, ^{1}H NMR, SEM, and DLS analyses of the resulting copolymers indicated formation of the nanoparticles in water. The formation of the one-handed helical conformation of the copolymer in both DMSO and water was confirmed by the CD spectra. An amphiphilic poly(*N*-propargylamide) containing fluorescent dyes was newly designed to evaluate cell uptake of nanoparticles of the amphiphilic copolymer by fluorescence microscopy. The *N*-propargylamide monomer **7**, having a rhodamine B dye moiety, was prepared and copolymerized with **1** and **5**. Human aortic endothelial cells (HAECs) were cultured in a medium containing the fluorescent-dye-labeled amphiphilic copolymer. Cell uptake of the copolymer was confirmed by red fluorescence emission from each of the HAECs. Progressive uptake was observed during the incubation period. When the cell culture experiment was conducted at 4 °C, the fluorescence intensity of the red emission was considerably lowered. This indicates that the cell uptake is inhibited at 4 °C and that this uptake process should occur in an endocytic pathway rather than by simple adsorption to the plasma membrane of HAECs. We are now synthesizing a fluorescent-dye-labeled hydrophilic copolymer of monomer **1** with monomer **7** to study preferential cell uptake of the nanoaggregates of the amphiphilic copolymer. In the future, we anticipate that nanoparticles will be able to be preferentially endocytosed into cells rather than monomeric chains of water-soluble copolymer. If this does occur, the nanoparticles of the amphiphilic copolymer will be a promising nanocarrier for drug delivery.

Acknowledgements: This work was financially supported by the *Asahi Glass Foundation*. The author (T. N.) thanks Professor *Mitsuru Akashi* of Osaka University and Dr. *Takami Akagi* of the Japan Science and Technology Agency for dynamic light scattering measurement. The author (T. N.) thanks Dr. *Tetsuji Yamaoka* and Dr. *Atsushi Mahara* of the National Cardiovascular Center Research Institute for fluorescence spectroscopy analysis.

[1] M. Okada, *Prog. Polym. Sci.* **2001**, *26*, 67
[2] Y. C. Lee, R. T. Lee, "*Neoglycoconjugates: Preparation and Applications*", Academic Press, San Diego **1994**.
[3] K. Kobayashi, A. Tsuchida, T. Usui, T. Akaike, *Macromolecules* **1997**, *30*, 2016.
[4] K. Kobayashi, N. Kakishita, M. Okada, T. Akaike, T. Usui, *J. Carbohydr. Chem.* **1994**, *13*, 753.
[5] L. L. Kiessling, N. L. Pohl, *Chem. Biol.* **1996**, *3*, 71.
[6] M.-G. Baek, R. C. Stevens, D. H. Charych, *Bioconjugate Chem.* **2000**, *11*, 777.
[7] I.-B. Kim, B. Erdogan, J. N. Wilson, U. H. F. Bunz, *Chem. Eur. J.* **2004**, *10*, 6247.
[8] T. Hasegawa, S. Kondoh, K. Matsuura, K. Kobayashi, *Macromolecules* **1999**, *32*, 6595.
[9] J. Kadokawa, Y. Shinmen, S. Shoda, *Macromol. Rapid Commun.* **2005**, *26*, 103.
[10] A. Takasu, K. Iso, T. Dohmae, T. Hirabayashi, *Biomacromolecules* **2006**, *7*, 411.
[11] K. Matsuura, S. Furuno, K. Kobayashi, *Chem. Lett.* **1998**, 847.
[12] J. Kadokawa, K. Tawa, M. Suenaga, Y. Kaneko, M. Tabata, *J. Macromol. Sci., Pure Appl. Chem.* **2006**, *43*, 1179.
[13] J. Deng, J. Tabei, M. Shiotsuki, F. Sanda, T. Masuda, *Macromolecules* **2004**, *37*, 9715 and references therein.
[14] R. R. Shrock, J. A. Osborn, *Inorg. Chem.* **1970**, *9*, 2339.
[15] J. Deng, J. Tabei, M. Shiotsuki, F. Sanda, T. Masuda, *Macromolecules* **2004**, *37*, 1891.
[16] M. Tabata, T. Sone, Y. Sadahiro, *Macromol. Chem. Phys.* **1999**, *200*, 265.
[17] J. Tabei, R. Nomura, T. Masuda, *Macromolecules* **2002**, *35*, 5405.
[18] G. Durin, S. Cottin, E. Blanc, A. R. Rees, *J. Temsamani, J. Biol. Chem.* **2003**, *278*, 31192.
[19] S. Muro, M. Koval, V. Muzykantov, *Curr. Vasc. Pharmacol.* **2004**, *2*, 281.

Cardiovasc Drugs Ther (2006) 20: 159–165
DOI 10.1007/s10557-006-8285-8

BASIC RESEARCH

Granulocyte Colony-Stimulating Factor Mediates Cardioprotection Against Ischemia/Reperfusion Injury via Phosphatidylinositol-3-Kinase/Akt Pathway in Canine Hearts

Hiroyuki Takahama · Tetsuo Minamino · Akio Hirata · Akiko Ogai · Hiroshi Asanuma · Masashi Fujita · Masakatsu Wakeno · Osamu Tsukamoto · Ken-ichiro Okada · Kazuo Komamura · Seiji Takashima · Yoshiro Shinozaki · Hidezo Mori · Naoki Mochizuki · Masafumi Kitakaze

Published online: 16 June 2006

Abstract
Purpose Recent studies suggest that G-CSF prevents cardiac remodeling following myocardial infarction (MI) likely through regeneration of the myocardium and coronary vessels. However, it remains unclear whether G-CSF administered at the onset of reperfusion prevents ischemia/reperfusion injury in the acute phase. We investigated acute effects of G-CSF on myocardial infarct size and the incidence of lethal arrhythmia and evaluated the involvement of the phosphatidylinositol-3 kinase (PI3K) in the *in vivo* canine models.
Methods In open-chest dogs, left anterior descending coronary artery (LAD) was occluded for 90 minutes followed by 6 hours of reperfusion. We intravenously administered G-CSF (0.33 μ/kg/min) for 30 minutes from the onset of reperfusion. Wortmannin, a PI3K inhibitor, was selectively administered into the LAD after the onset of reperfusion.
Results G-CSF significantly ($p < 0.05$) reduced myocardial infarct size (38.7±4.3% to 15.7±5.3%) and the incidence of ventricular fibrillation during reperfusion periods (50% to 0%) compared with the control. G-CSF enhanced Akt phospholylation in ischemic canine myocardium. Wortmannin blunted both the infarct size-limiting and anti-arrhythmic effects of G-CSF. G-CSF did not change myeloperoxidase activity, a marker of neutrophil accumulation, in the infarcted myocardium.
Conclusion An intravenous administration of G-CSF at the onset of reperfusion attenuates ischemia/reperfusion injury through PI3K/Akt pathway in the *in vivo* model. G-CSF administration can be a promising candidate for the adjunctive therapy for patients with acute myocardial infarction.

Takahama and Hirata contributed equally to this work.

H. Takahama · A. Ogai · H. Asanuma · M. Wakeno · K. Komamura · H. Mori · M. Kitakaze
Department of Cardiovascular Medicine,
National Cardiovascular Center,
Suita 565-8565, Osaka, Japan

H. Takahama · M. Wakeno · N. Mochizuki
Department of Structural Analysis,
National Cardiovascular Center,
Suita 565-8565, Osaka, Japan

H. Takahama · M. Wakeno · N. Mochizuki
Department of Bioregulatory Medicine,
Osaka University Graduate School of Medicine,
Suita 565-0871, Osaka, Japan

T. Minamino (✉) · A. Hirata · M. Fujita · O. Tsukamoto · K.-i. Okada · S. Takashima
Department of Cardiovascular Medicine,
Osaka University Graduate School of Medicine,
2-2 Yamadaoka, Suita 565-0871, Osaka, Japan
e-mail: minamino@medone.med.osaka-u.ac.jp

Y. Shinozaki
Department of Physiological Science,
Tokai University School of Medicine,
Isehara 259-1193, Kanagawa, Japan

Key words G-CSF · myocardial infarction · ischemia-reperfusion injury · ventricular fibrillation · phosphatidylinositol-3 kinase · Akt

Abbreviations

VF	ventricular fibrillation
G-CSF	granulocyte colony-stimulating factor
WTMN	wortmannin

Introduction

Granulocyte colony-stimulating factor (G-CSF), a 20-kDa glycoprotein, promotes the proliferation, survival and differentiation of hematopoietic cells [1]. Furthermore, G-CSF can mobilize hematopoietic stem cells from bone marrow [2, 3]. Thus, G-CSF is believed to improve cardiac remodeling after myocardial infarction (MI) through regeneration of the myocardium and angiogenesis [4, 5]. In addition to these effects of G-CSF, Komuro and colleagues clearly demonstrated that the high dose of G-CSF acutely reduces infarct size by preventing apoptosis in the isolated hearts [6]. However, it remains unclear whether clinically relevant dosages of G-CSF can reduce the infarct size in the in vivo model and, if so, it is not clear which downstream signaling pathway is involved in the acute cardioprotective effects of G-CSF. Furthermore, although lethal arrhythmias are a major cause of death in patients with acute myocardial infarction [7, 8], anti-arrhythmic effects of G-CSF have not been determined.

Thus, we investigated the acute effects of a clinical relevant dose of G-CSF on ischemia/reperfusion injury including both lethal arrhythmias and infarct size in canine hearts. We also examined a role of the PI3K/Akt pathway, a down stream of G-CSF receptors, in the cardioprotective effects of G-CSF. In the present study, we adopted ischemia/reperfusion protocols that have not been tested in previous studies [4, 5], because coronary revascularization has been established as a standard therapy to attenuate cardiac damage after MI.

Materials and methods

Materials

G-CSF was provided by Kirin brewery company (Tokyo, Japan). Recombinant human G-CSF can increase the number of white blood cells in dogs [9]. Wortmannin was obtained from Sigma (St. Louis, MO), and antibodies against Phospho-Akt and Akt were obtained from Cell signaling technologies (Beverly, MA).

Instrumentation

Twenty-nine beagle dogs (Kitayama Labes, Gifu, Japan) weighing 8 to 12 kg were anesthetized by an intravenous injection of sodium pentobarbital (30 mg/kg), intubated and ventilated with room air mixed with oxygen (100% O_2 at flow rate of 1.0 to 1.5 l/min). Thoracotomy was done at the fifth left intercostal space, and the heart was suspended in a pericardial cradle. After intravenous administration of heparin (500 U/kg), the left anterior descending coronary artery (LAD) was cannulated for perfusion with blood from the left carotid artery through an extracorporeal bypass tube. This allows the selective infusion of drugs into the LAD-perfused areas through this bypass tube. The left atrium was catheterized for microsphere injection to measure myocardial collateral blood flow during ischemia as described previously [10]. Hydration was maintained by a slow normal saline infusion. Both systemic blood pressure (SBP) and heart rate (HR) were monitored continuously during the study. All procedures were performed in conformity with the Guide for the care and use of laboratory animals (NIH Publication No. 85–23, 1996 revision), and were approved by the *Osaka University Committee for Laboratory Animal Use.*

Experimental protocols

Protocol 1. Acute effects of G-CSF on infarct size and lethal arrhythmias in canine hearts

After hemodynamic stabilization, we intravenously administered either saline (Control group; $n = 9$) or G-CSF (0.33 μg/kg/min) (G-CSF group; $n = 6$) for 30 min following the onset of reperfusion. An intracoronary administration of wortmannin (WTMN), a PI3K inhibitor, was selectively administered into the LAD (1.5 μg/kg/min) for 60 min after the onset of reperfusion (GCSF + WTMN group, $n = 7$; WTMN group, $n = 7$) (Fig. 1). We have previously confirmed that the dose of wortmannin used prevents the phosphorylation of Akt in myocardium [10]. We measured infarct size and myocardial collateral blood flow during ischemia. In brief, infarct size was evaluated at the end of the protocol by Evans blue/TTC staining. Collateral blood flow during 90 min of ischemia was assessed by the non-radioactive microsphere method [10]. We also counted

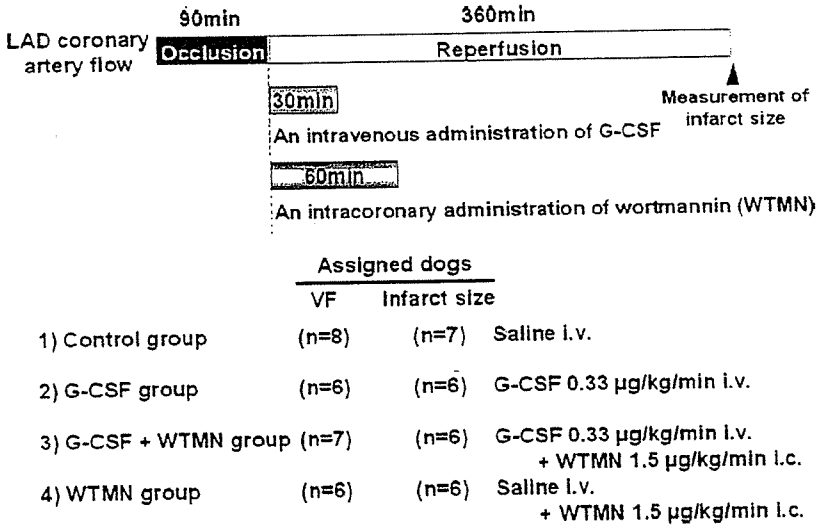

Fig. 1 Experimental protocols to assess myocardial infarct size and ventricular fibrillation (VF) in canine hearts. Myocardial infarct size was measured after 90 min of left anterior descending coronary artery (LAD) occlusion followed by 360 min of reperfusion. The incidence of VF was evaluated during reperfusion for 360 min. Intravenous administration of granulocyte colony-stimulating factor (G-CSF) was started at the onset of reperfusion and continued for 30 min. Intracoronary administration of wortmannin (WTMN) was started at the onset of reperfusion and continued for 60 min.

the incidence of VF during the 6 h reperfusion period (Fig. 1).

Finally, we measured myeloperoxidase (MPO) activity in LAD-perfused myocardium to check the accumulation of neutrophils in infarcted myocardium.

Protocol 2. Phosphorylation of Akt in ischemic myocardium

In this protocol, we used 11 dogs in Control group (n = 3), G-CSF group (n = 4), and G-CSF + WTMN group (n = 4). After 90 min of ischemia followed by 30 min of reperfusion, hearts were excised. The myocardial tissue in the ischemic zone, which was identified as the edge of the region showing necrosis, and non-ischemic zone were quickly placed into liquid nitrogen and stored at −80°C. Phosphorylation of Akt and total content of Akt were evaluated by immunoblotting as reported previously [10].

Immunoblotting

Immunoblotting was performed as described previously [11], and the immunoreactive bands were quantified by densitometry (Molecular Dynamics).

MPO activity

Several myocardial tissue samples were taken from the ischemic area in the dogs studied, frozen in liquid nitrogen and stored at −80°C until assay. The technical procedure has been described previously [12]. One unit of MPO activity was defined as that which degrades 1 μmol hydrogen peroxide per minute at 25°C.

Statistical analysis

Results are expressed as the mean ± SEM. Comparisons of the time course of the change in mean SBP and HR between groups were performed using two-way repeated measures analysis of variance (ANOVA). Comparisons of other data between groups were performed using one-way factional ANOVA. The Bonferroni-Holm procedure was used for correction of multiple comparisons [13]. The incidence of VF was compared using the χ^2-test and Fisher's exact probability test. A p value < 0.05 was considered to represent statistical significance.

Results

Criteria for exclusion

Since there was a negative correlation between myocardial collateral blood flow during ischemia and the incidence of VF [14, 15], it was important to assess myocardial collateral blood flow and exclude the dogs with high myocardial collateral blood flow. We excluded two dogs with excessive collateral blood flow (>15 ml/100 g/min) (Control group: 1, WTMN group: 1) among 29 dogs tested. Thus, 27 dogs were

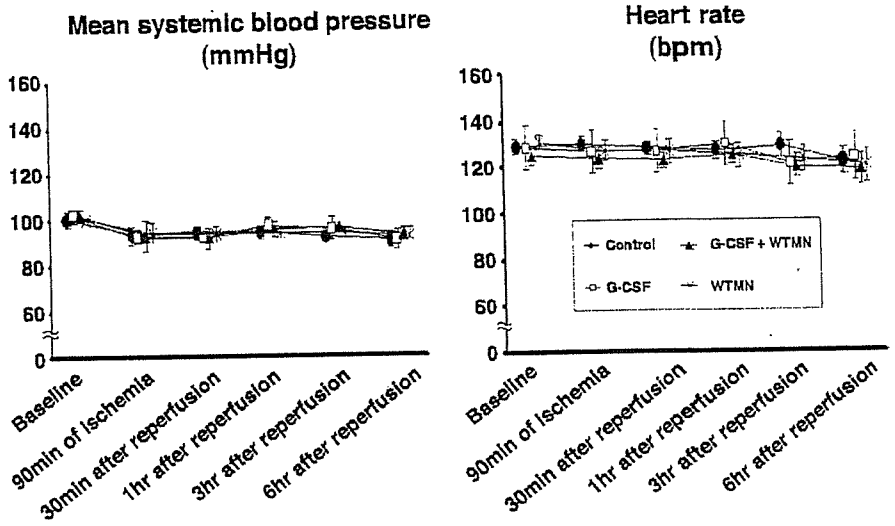

Fig. 2 The changes in mean systemic blood pressure (SBP) and heart rate (HR) during the experiment in groups tested. Neither SBP nor HR differed between the groups tested at baseline, 90 min of ischemia, at 30 min and 1, 3, and 6 h after reperfusion.

evaluated for VF analysis. Among these 27 dogs, we further excluded two dogs (Control group: 1, G-CSF + WTMN group: 1) from infarct size analysis that matched the exclusion criteria of lethal arrhythmia (more than two consecutive attempts required to convert VF with low-energy DC pulses applied directly to the heart) [10].

Effects of G-CSF on infarct size and VF during the reperfusion period

Throughout the study, neither SBP nor HR differed among the four groups (Fig. 2). The area at risk and myocardial collateral blood flow during myocardial ischemia were also comparable in the groups tested (Fig. 3). Figure 4 shows infarct size in the groups tested. G-CSF reduced ($p < 0.05$) infarct size compared with the control group. The intracoronary administration of wortmannin for 60 min after the onset of reperfusion abrogated the infarct size-limiting effects of G-CSF, although wortmannin alone did not affect infarct size.

G-CSF reduced ($p < 0.05$) the incidence of VF during the reperfusion period compared with the control group (Table 1). The antiarrhythmic effects of G-CSF were abolished by wortmannin.

Effect of G-CSF on MPO activity in infarcted myocardium

MPO activity in infarcted myocardium 6 h after reperfusion in G-CSF group did not differ from that in the control group. (10.0 ± 2.6 versus 10.7 ± 2.1 U/g protein).

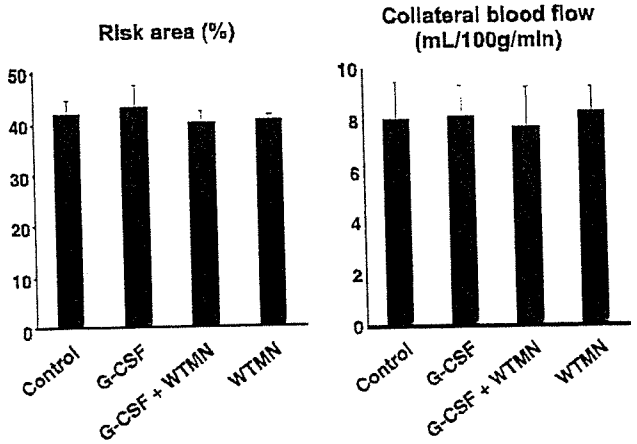

Fig. 3 Area at risk and myocardial collateral blood flow during ischemia in groups tested. Neither the area at risk nor myocardial collateral blood flow differed between the groups tested.

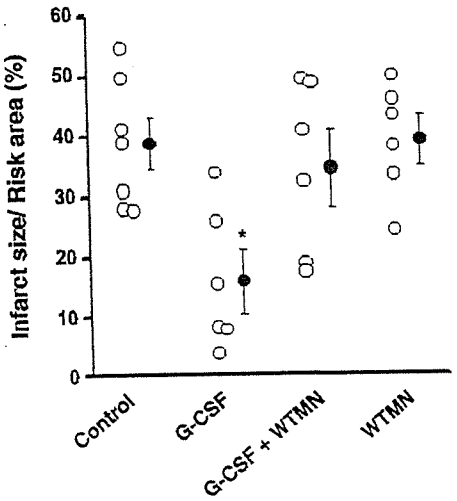

Fig. 4 Infarct size as a percentage of the area at risk in groups tested. Intravenous administration of G-CSF limited infarct size. The infarct-size limiting effect of G-CSF was blunted by the intracoronary administration of WTMN during reperfusion. *$p <$ 0.05 vs. control group.

Table 1 Effects of G-CSF on the incidence of VF during reperfusion periods

Group	Incidence of VF (%)	
Control	50.0	(4/8)
G-CSF	0*	(0/6)
G-CSF + WTMN	42.9	(3/7)
WTMN	50.0	(3/6)

*$p < 0.05$ vs. control group

Effect of G-CSF on Akt phosphorylation in ischemic myocardium

G-CSF augmented Akt phosphrylation in the LAD-perfused myocardium. The increase in Akt phosphorylation was attenuated by wortmannin (Fig. 5).

Discussion

The present study demonstrated that administration of G-CSF following the onset of reperfusion limited infarct size in acute phase and reduced the incidence of lethal arrhythmia. The intracoronary administration of wortmannin abrogated these cardioprotective effects of G-CSF, suggesting that G-CSF mediated cardioprotection via the PI3K/Akt pathway. To our knowledge, this is the first study to reveal the acute effect of G-CSF against ischemia/reperfusion injury via the PI3K/Akt pathway in in vivo canine hearts.

Previous studies have reported that G-CSF improves cardiac remodeling after MI in the chronic ligation model of coronary artery [4, 5, 16]. It has been believed that G-CSF exerts cardioprotective effects through regeneration of myocardium and angiogenesis. Recently, Komuro and colleagues clearly demonstrated that the high dose of G-CSF limits infarct size in the acute phase in the isolated hearts [6]. To translate their remarkable findings into the clinical setting, we need to consider the dose of G-CSF and experimental models in their study. They used a perfusate containing 300 ng/ml G-CSF in the isolated heart model. This dose is relatively high compared with the dose used in clinical settings [17, 18]. In addition, effects of G-CSF on neutrophil function cannot be tested in the isolated heart model. In the present study, we demonstrated that a clinical relevant dose of G-CSF acutely limits infarct size in the in vivo model. In contrast with previous studies [4, 5, 16], we examined the effects of G-CSF in the ischemia/reperfusion model, because coronary revascularization is principally applied for patients with acute MI to attenuate ischemia/reperfusion injury. We found that G-CSF following the onset of reperfusion effectively limited infarct size. Our findings strongly support that G-CSF would be a promising candidate as an adjunctive therapy for patients with acute MI. Indeed, two recent publications by the FIRSTLINE-AMI trial clearly demonstrated that subcutaneous administration of G-CSF after percutaneous coronary intervention improved cardiac function and prevented cardiac remodeling [19, 20]. Considering our present data, the improvement of cardiac function by G-CSF in clinical studies will be due to limiting infarct size in the acute phase as well as preventing cardiac remodeling.

G-CSF can provoke multiple intracellular signal transductions including Jak/Stat, ERK and PI3K/Akt [16, 21]. Recently, we and others demonstrated that post-interventions which activate PI3K/Akt during the reperfusion protect against ischemia/reprfusion injury [10, 22]. Thus, we investigated a role of PI3K/Akt in G-CSF-mediated cardioprotection. WTMN significantly blunted the infarct size-limiting effects of G-CSF, and G-CSF enhanced Akt phosphorylation in the ischemic myocardium, indicating that G-CSF reduces infarct size via PI3K/Akt-dependent pathway. Further investigations will be needed to clarify the molecular target of PI3K/Akt and the role of other signals activated by G-CSF in this condition.

Although we demonstrated that G-CSF mediated cardioprotection, one small clinical study showed that G-CSF may induce coronary re-stenosis [23]. In contrast, other large-scale studies did not show that G-CSF induced coronary restenosis [19, 20]. Since there is still controversy about the restenosis effects of G-

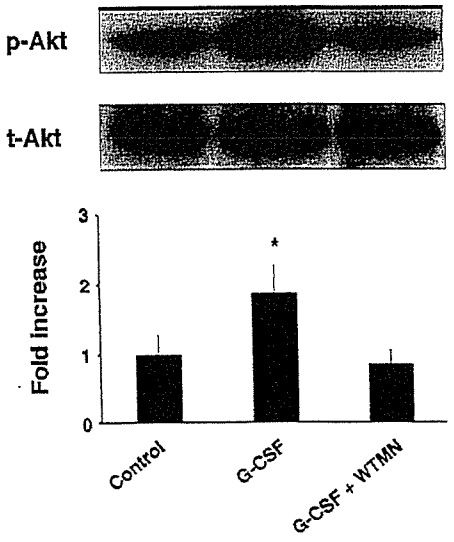

Fig. 5 Akt phosphorylation in LAD-perfused areas. G-CSF phosphorylated Akt in LAD-perfused myocardium. Akt phosphorylation by G-CSF was prevented by co-treatment with WTMN. Akt phosphorylation was normalized by total Akt. *$p < 0.05$ vs. control group.

CSF, this issue will be minimized by the concomitant use of a drug-eluting stent and G-CSF. Another possible adverse effect of G-CSF will be enhancement of neutrophil function. G-CSF appears not only to stimulate the formation of granulocyte colonies from bone marrow-derived precursors, but also to enhance the function of mature neutrophils [24] and elevates the number of white blood cells, which may predict adverse prognosis in the patients of acute MI [25]. Consistent with previous studies [26, 27], we also showed that G-CSF did not change MPO activity, a marker of neutrophil accumulation, in the infarcted myocardium. These findings suggest that G-CSF exerted cardioprotective effects independent of white blood cells. Although our findings suggest that the overall effect of G-CSF may be beneficial for ischemia/reperfused myocardium, we need to be cautious about these potential adverse effects of G-CSF.

Importantly, we clearly demonstrated that G-CSF reduced the incidence of VF during reperfusion via the PI3/Akt-dependent pathway. Since lethal arrhythmias are one of the major causes of death in patients with acute MI [8], the anti-arrhythmic effects of G-CSF have great clinical impact. We have previously demonstrated that another cytokine, erythropoietin, also reduced the incidence of lethal arrhythmia via the PI3/Akt pathway [10]. Although our findings suggest that the PI3K/Akt-dependent pathway will play an important role in the generation of lethal arrhythmias, further investigation will be needed to clarify the potential mechanism by which G-CSF exerts anti-arrhythmic effects. We need to consider whether G-CSF exerts anti-arrhythmic effects by the reduction of myocardial infarct size or by some other actions of G-CSF.

In conclusion, the intravenous administration of a clinically relevant dose of G-CSF will be a promising strategy to treat patients with acute MI. Further controlled studies will be warranted to check the safety and efficacy of G-CSF treatment in the acute phase after MI.

Acknowledgments We thank Yuko Okuda, and Yoko Nagamachi for their technical assistance.

References

1. Clark SC, Kamen R. The human hematopoietic colony-stimulating factors. Science 1987;236:1229–37.
2. To LB, Haylock DN, Simmons PJ, Juttner CA. The biology and clinical uses of blood stem cells. Blood 1997;89:2233–58.
3. Kronenwett R, Martin S, Haas R. The role of cytokines and adhesion molecules for mobilization of peripheral blood stem cells. Stem Cells 2000;18:320–30.
4. Orlic D, Kajstura J, Chimenti S, et al. Mobilized bone marrow cells repair the infarcted heart, improving function and survival. Proc Natl Acad Sci USA 2001;98:10344–9.
5. Ohtsuka M, Takano H, Zou Y, et al. Cytokine therapy prevents left ventricular remodeling and dysfunction after myocardial infarction through neovascularization. Faseb J 2004;18:851–3.
6. Harada M, Qin Y, Takano H, et al. G-CSF prevents cardiac remodeling after myocardial infarction by activating the Jak-Stat pathway in cardiomyocytes. Nat Med 2005;11:305–11.
7. Nicod P, Gilpin E, Dittrich H, et al. Late clinical outcome in patients with early ventricular fibrillation after myocardial infarction. J Am Coll Cardiol 1988;11:464–70.
8. Rouleau JL, Talajic M, Sussex B, et al. Myocardial infarction patients in the 1990s—their risk factors, stratification and survival in Canada: the Canadian Assessment of Myocardial Infarction (CAMI) Study. J Am Coll Cardiol 1996;27:1119–27.
9. Lothrop CD Jr, Warren DJ, Souza LM, Jones JB, Moore MA. Correction of canine cyclic hematopoiesis with recombinant human granulocyte colony-stimulating factor. Blood 1988;72:1324–8.
10. Hirata A, Minamino T, Asanuma H, et al. Erythropoietin just before reperfusion reduces both lethal arrhythmias and infarct size via the phosphatidylinositol-3 kinase-dependent pathway in canine hearts. Cardiovasc Drugs Ther 2005;19:33–40.
11. Maruyama R, Takemura G, Aoyama T, et al. Dynamic process of apoptosis in adult rat cardiomyocytes analyzed using 48-hour videomicroscopy and electron microscopy: beating and rate are associated with the apoptotic process. Am J Pathol 2001;159:683–91.
12. Asanuma H, Kitakaze M, Funaya H, et al. Nifedipine limits infarct size via NO-dependent mechanisms in dogs. Basic Res Cardiol 2001;96:497–505.
13. Holm S. A simple sequentially rejective multiple test procedure. Scand J Statist 1979;6:65–70.
14. Hale SL, Lange R, Alker KJ, Kloner RA. Correlates of reperfusion ventricular fibrillation in dogs. Am J Cardiol 1984;53:1397–400.
15. Bolli R, Patel B. Factors that determine the occurrence of reperfusion arrhythmias. Am Heart J 1988;115:20–9.
16. Iwanaga K, Takano H, Ohtsuka M, et al. Effects of G-CSF on cardiac remodeling after acute myocardial infarction in swine. Biochem Biophys Res Commun 2004;325:1353–9.
17. Gabrilove JL, Jakubowski A, Fain K, et al. Phase I study of granulocyte colony-stimulating factor in patients with transitional cell carcinoma of the urothelium. J Clin Invest 1988; 82:1454–61.
18. Bensinger WI, Clift RA, Anasetti C, et al. Transplantation of allogeneic peripheral blood stem cells mobilized by recombinant human granulocyte colony stimulating factor. Stem Cells 1996;14:90–105.
19. Ince H, Petzsch M, Kleine HD, et al. Prevention of left ventricular remodeling with granulocyte colony-stimulating factor after acute myocardial infarction: final 1-year results of the Front-Integrated Revascularization and Stem Cell Liberation in Evolving Acute Myocardial Infarction by Granulocyte Colony-Stimulating Factor (FIRSTLINE-AMI) Trial. Circulation 2005;112:I73–80.
20. Ince H, Petzsch M, Kleine HD, et al. Preservation from left ventricular remodeling by front-integrated revascularization and stem cell liberation in evolving acute myocardial infarction by use of granulocyte-colony-stimulating factor (FIRSTLINE-AMI). Circulation 2005;112:3097–106.
21. Avalos BR. Molecular analysis of the granulocyte colony-stimulating factor receptor. Blood 1996;88:761–77.

22. Tsang A, Hausenloy DJ, Mocanu MM, Yellon DM. Post-conditioning: a form of "modified reperfusion" protects the myocardium by activating the phosphatidylinositol 3-kinase-Akt pathway. Circ Res 2004;95:230–2.
23. Kang HJ, Kim HS, Zhang SY, et al. Effects of intracoronary infusion of peripheral blood stem-cells mobilised with granulocyte-colony stimulating factor on left ventricular systolic function and restenosis after coronary stenting in myocardial infarction: the MAGIC cell randomised clinical trial. Lancet 2004;363:751–6.
24. Weisbart RH, Golde DW, Clark SC, Wong GG, Gasson JC. Human granulocyte-macrophage colony-stimulating factor is a neutrophil activator. Nature 1985;314:361–3.
25. Barron HV, Cannon CP, Murphy SA, Braunwald E, Gibson CM. Association between white blood cell count, epicardial blood flow, myocardial perfusion, and clinical outcomes in the setting of acute myocardial infarction: a thrombolysis in myocardial infarction 10 substudy. Circulation 2000;102: 2329–34.
26. Adachi Y, Imagawa J, Suzuki Y, et al. G-CSF treatment increases side population cell infiltration after myocardial infarction in mice. J Mol Cell Cardiol 2004;36: 707–10.
27. Sugano Y, Anzai T, Yoshikawa T, et al. Granulocyte colony-stimulating factor attenuates early ventricular expansion after experimental myocardial infarction. Cardiovasc Res 2005;65:446–56.

The EMBO Journal (2006) 25, 2388–2396 | © 2006 European Molecular Biology Organization | All Rights Reserved 0261-4189/06
www.embojournal.org

THE EMBO JOURNAL

Crystal structures of VAP1 reveal ADAMs' MDC domain architecture and its unique C-shaped scaffold

Soichi Takeda[1,2,*], Tomoko Igarashi[1], Hidezo Mori[1] and Satohiko Araki[3]

[1]Department of Cardiac Physiology, National Cardiovascular Center Research Institute, Suita, Osaka, Japan, [2]Laboratory for Structural Biochemistry, Riken Harima Institute at SPring-8, Mikazuki, Sayo, Hyogo, Japan and [3]Sugashima Marine Biological Laboratory, Graduate School of Science, Nagoya University, Toba, Mie, Japan

ADAMs (a disintegrin and metalloproteinase) are sheddases possessing extracellular metalloproteinase/disintegrin/cysteine-rich (MDC) domains. ADAMs uniquely display both proteolytic and adhesive activities on the cell surface, however, most of their physiological targets and adhesion mechanisms remain unclear. Here for the first time, we reveal the ADAMs' MDC architecture and a potential target-binding site by solving crystal structures of VAP1, a snake venom homolog of mammalian ADAMs. The D-domain protrudes from the M-domain opposing the catalytic site and constituting a C-shaped arm with cores of Ca^{2+} ions. The disintegrin-loop, supposed to interact with integrins, is packed by the C-domain and inaccessible for protein binding. Instead, the hyper-variable region (HVR) in the C-domain, which has a novel fold stabilized by the strictly conserved disulfide bridges, constitutes a potential protein–protein adhesive interface. The HVR is located at the distal end of the arm and faces toward the catalytic site. The C-shaped structure implies interplay between the ADAMs' proteolytic and adhesive domains and suggests a molecular mechanism for ADAMs' target recognition for shedding.

The EMBO Journal (2006) **25**, 2388–2396. doi:10.1038/sj.emboj.7601131; Published online 11 May 2006
Subject Categories: signal transduction; structural biology
Keywords: ADAM; MDC; protein–protein interaction shedding; snake venom metalloproteinase

Introduction

ADAMs (a disintegrin and metalloproteinase) or MDC (metalloproteinase/disintegrin/cysteine-rich) proteins comprise an emerging class of mammalian metalloproteinases with potential regulatory roles in cell–cell and cell–matrix adhesion and signalling (Becherer and Blobel, 2003; Seals and Courtneidge, 2003; White, 2003; Blobel, 2005). To date, over 30 ADAMs have been identified in a variety of species from fission yeast to human. Roughly, half of these are believed to function as active metalloproteinases and thus to constitute major membrane-bound sheddase that can proteolytically release cell-surface-protein ectodomains including growth factors and cytokines, their receptors and cell adhesion molecules. For example, ADAM17 (TACE, TNF-α converting enzyme) releases many cell-surface proteins including TNF-α precursor (Black *et al*, 1997; Moss *et al*, 1997) and ADAM10 (kuzbanian), which dictates lateral inhibition of *Drosophila* neurogenesis (Rooke *et al*, 1996), releases Notch ligand Delta (Qi *et al*, 1999) and Notch itself (Pan and Rubin, 1997). With regard to cellular interactions, fertilin α and β (ADAM1 and ADAM2, respectively) have been identified as sperm surface molecules essential for fertilization (Primakoff *et al*, 1987; Blobel *et al*, 1990, 1992) and meltrin α (ADAM12) is implicated in myogenesis (Yagami-Hiromasa *et al*, 1995). ADAMs have been associated with numerous diseases including arthritis, Alzheimer's disease, and cancer (Duffy *et al*, 2003; Moss and Bartsch, 2004). ADAM33 has been genetically linked with asthma (Van Eerdewegh *et al*, 2002). ADAMs uniquely display both proteolytic and adhesive activities on the cell surface, however, most of their physiological targets and the adhesion mechanisms remain unclear.

Disintegrins are small proteins (40–90 aa) isolated from snake venom typically with an Arg-Gly-Asp (RGD) recognition sequence on an extended loop (disintegrin-loop) that inhibit platelet aggregation via integrin binding (Huang *et al*, 1987; Calvete *et al*, 2005). ADAMs are unique among cell surface proteins in possessing a disintegrin (D-) domain and thus it has been suggested that integrins might be common receptors for ADAMs (Blobel *et al*, 1992; Evans, 2001; White, 2003). However, the RGD sequence in the ADAMs' disintegrin-loop is usually replaced by XXCD and therefore, its adhesive potential has been controversial. Both the ADAMs' D- and cysteine-rich (C-) domains are involved in the protein–protein interactions (Myles *et al*, 1994; Almeida *et al*, 1995; Zolkiewska, 1999; Iba *et al*, 2000; Gaultier *et al*, 2002; Smith *et al*, 2002), however, the details of the interactions have remained elusive. This is because high-resolution structures have been available only for isolated domains (Maskos *et al*, 1998; Orth *et al*, 2004; Janes *et al*, 2005) and no structural information has been available for the C-domain of the canonical ADAMs. To clarify the molecular mechanisms of target recognition for shedding by and of cellular adhesion via ADAMs, elucidation of the atomic structure of the ADAMs' MDC domains is indispensable.

To obtain structural data on an ADAM family member, we exploited the fact that hemorrhagic P-III snake venom metalloproteinases (SVMPs) share the ADAMs' MDC architecture (Jia *et al*, 1996; Evans, 2001; Fox and Serrano, 2005). Most ADAMs possess additionally, EGF-like, transmembrane and cytoplasmic domains and therefore are primarily membrane-associated, whereas SVMPs are secreted. Vascular apoptosis-inducing protein-1 (VAP1) is a disulfide-bridged

*Corresponding author. Department of Cardiac Physiology, National Cardiovascular Center Research Institute, Fujishirodai 5-7-1, Suita, Osaka, 565-8565, Japan. Tel.: +81 6 6833 5012 ext.2381; Fax: +81 6 6872 7485; E-mail: stakeda@ri.ncvc.go.jp

Received: 17 February 2006; accepted: 12 April 2006; published online: 11 May 2006

homodimer P-III SVMP isolated from *Crotalus atrox* venom (Masuda *et al*, 1998, 2000). VAP1's stability and intrinsic two-fold symmetry enabled us to solve the crystal structures at 2.5-Å resolution. The structure reveals the residues that are important for stabilizing the MDC architecture are strictly conserved throughout the primary structure among all the known ADAMs. Therefore, the present structure represents the general architecture of ADAMs' MDC domains and provides insights into the molecular mechanism of the ADAMs' target recognition.

Results

Structure determination

VAP1 yielded crystals readily, and initial phases were determined by molecular replacement method using the structure of P-I SVMP, acutolysin-C (1QUA) (Zhu *et al*, 1999) as a starting model. Although the initial model, with 99 identical residues out of 197, represented less than 50% of the total molecule, two distinct local noncrystallographic two-fold symmetry (NCS) operations (see below) allowed us to completely model the whole molecule. The native structures were determined from the crystals with two distinct space groups, $P2_12_12_1$ and $P4_12_12$, both at 2.5-Å resolution (Table I). Orthorhombic crystals were used for inhibitor soaking and the GM6001 ((3-(*N*-hydroxycarboxamido)-2-isobutyl-propanoyl-Trp-methylamide))-bound structure was determined at 3.0-Å resolution (Table I). In either crystal forms, the asymmetric unit contained one dimer molecule. The four monomers in the two crystal forms have almost identical structures, except for slight variations in their domain orientations, terminal residues, surface loops and active-site GM6001-binding region.

MDC architecture

The MDC architecture of VAP1 is shown in Figure 1A and B. The metalloproteinase (M-) domains in the dimer are related by NCS such that their active sites point in opposite directions and an intermolecular disulfide bridge is formed between symmetry-related Cys365 residues (Figure 1A). The M-domain is followed by a disintegrin (D-) domain that is further divided into D_s- and D_a-domains (see below). The D_s-domain protrudes from the M-domain close to the Ca^{2+}-binding site I (see below) opposing the catalytic site. The D-domain forms a C-shaped arm, together with the cysteine-rich (C-) domain, with its concave surface toward the M-domain. There are no direct interactions between the arm and the M-domain. Notably, the distal portion of the C-domain comes close to

Table I Data collection and refinement statistics

	Native (orthorhombic)	Native (tetragonal)	GM6001-bound
Data collection			
Space group	$P2_12_12_1$	$P4_12_12$	$P2_12_12_1$
Cell dimensions			
a, *b*, *c* (Å)	86.7, 93.3, 137.7	93.9,93.9,244.8	86.3, 91.4, 136.0
α, β, γ (deg)	90, 90, 90	90, 90, 90	90, 90, 90
Resolution (Å)	50–2.50 (2.59–2.50)	50–2.50 (2.59–2.50)	50–2.95 (3.06–2.95)
R_{merge}[a]	0.072 (0.369)	0.084 (0.380)	0.072 (0.367)
$I/\sigma I$	14.4 (2.9)	18.7 (7.1)	12.6 (4.3)
Completeness (%)	99.4 (98.8)	99.7 (99.6)	99.9 (99.4)
Redundancy	3.91	12.7	4.95
Refinement			
Resolution (Å)	50–2.50 (2.59–2.50)	50–2.50 (2.59–2.50)	50–2.95 (3.06–2.95)
No. of reflections	38874	38786	23295
R_{work}[b]/R_{free}[c]	0.212/0.258	0.229/0.269	0.208/0.264
No. of atoms			
Protein	6558	6513	6558
Zn^{2+}	2	2	2
Ca^{2+}	4	4	4
Co^{3+}	1		1
N-acetyl glucosamine	56	42	56
GM6001			56
Water	205	165	35
B-factors			
Protein	44.9	51.2	55.4
Zn^{2+}	40.9	41.6	46.4
Ca^{2+}	43.5	52.4	49.3
Co^{3+}	35.5		56.8
N-acetyl glucosamine	69.8	65.1	75.8
GM6001			78.6
Water	39.8	41.5	37.0
R.m.s deviations			
Bond lengths (Å)	0.0052	0.0080	0.0038
Bond angles (deg)	1.18	1.39	0.92

[a] $R_{merge} = \sum_{hkl}\sum_i|I_i(hkl) - \langle I(hlk)\rangle| / \sum_{hkl}\sum_i I_i(hkl)$, where $I_i(hkl)$ is the ith intensity measurement of reflection *hkl* and $\langle I(hlk)\rangle$ is its average.
[b] $R_{work} = \sum(||F_{obs}| - |F_{calc}||)/\sum|F_{obs}|$.
[c] R_{free} = *R*-value for a randomly selected subset (5%) of the data that were not used for minimization of the crystallographic residual.
Highest resolution shell is shown in parenthesis.
For each data set, single crystal was used for measurement.

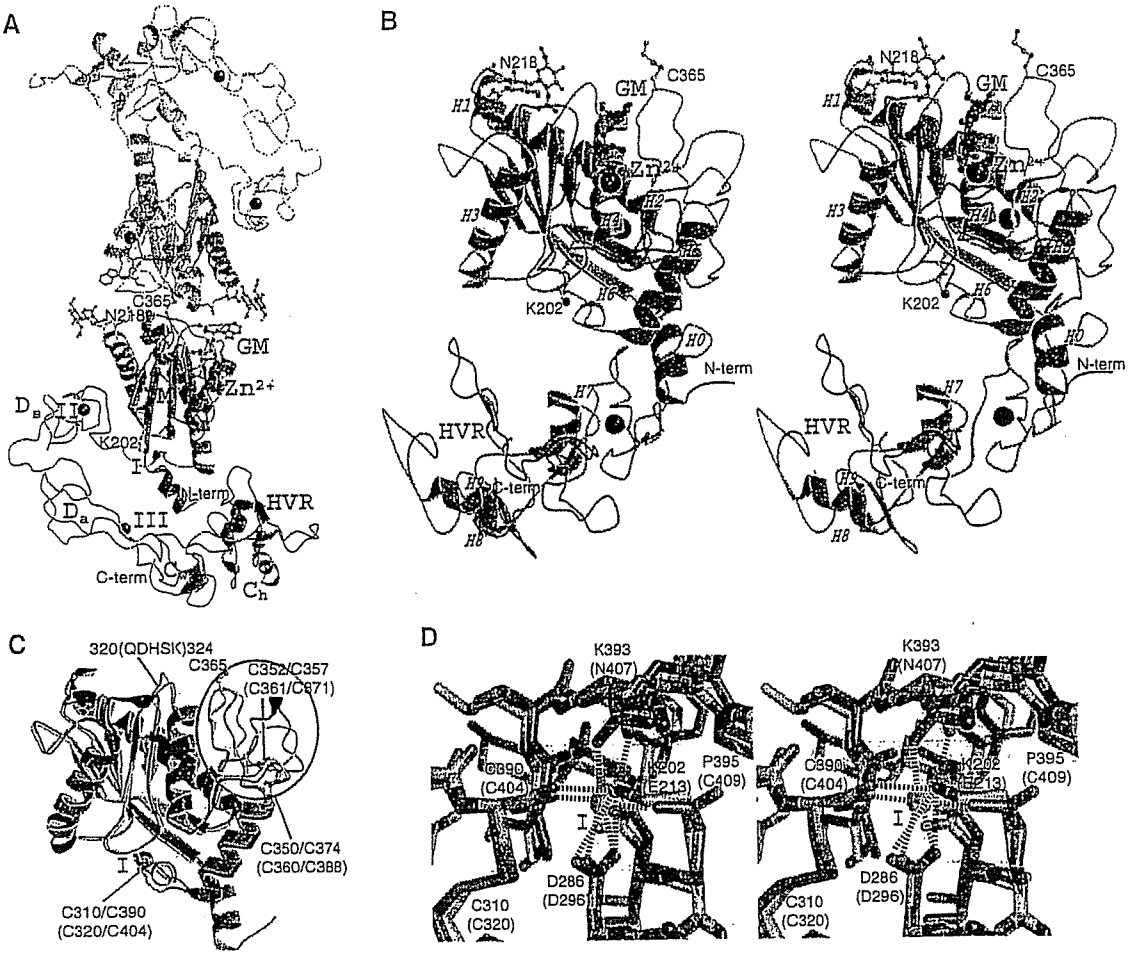

Figure 1 MDC architecture. (A) VAP1 dimer viewed from the NCS axis. The H0-helix, M-domain, linker, D_s-, D_a-, C_w-, and C_h-domains and HVRs belonging to the one monomer are shown in red, yellow, gray, cyan, pink, gray, green and blue, respectively. The disulfide-linked counterpart is shown in gray. Zinc and calcium ions are represented as red and black spheres, respectively. The NAG (*N*-acetyl-glucosamine, in orange) moieties linked to Asn218, the calcium-mimetic Lys202 and the bound inhibitor GM6001 (GM, in green) are in ball-stick representations. (B) Stereo view of VAP1 monomer from the direction nearly perpendicular to (A). The helix numbers are labelled. (C) Superposition of the M-domains of ADAM33 (blue) and VAP1 (yellow). The calcium ion bound to site I and the zinc ion in ADAM33 are represented by black and red spheres, respectively. The disulfide bridges are indicated in black and blue letters for VAP1 and ADAM33, respectively. The QDHSK sequence for the dimer interface in VAP1 (residues 320–324) is in red. (D) Comparison of the calcium-binding site I structures of ADAM33 (blue) and VAP1 (yellow) *in stereo*. The residues in ADAM33 and in VAP1 are labelled in blue and black, respectively. A calcium ion and a water molecule bound to ADAM33 are represented as green and red spheres, respectively. The ammonium group of Lys202 in VAP1 occupies the position of the calcium ion in ADAM33. In ADAM33 (Orth *et al*, 2004), side-chain oxygen atoms of Glu213, Asp296 and Asn407, the carbonyl oxygen of Cys404 and a water molecule form the corners of a pentagonal bipyramid and ligand to the calcium ion.

and faces toward the catalytic site in the M-domain. The C-terminus Tyr610 is located proximal to the boundary between the D_a- and C-domains (Figure 1A and B). Aside from Cys365, each monomer contains 34 cysteinyl residues, all of which are involved in disulfide bonding, and their spacings are strictly conserved among ADAMs (Figure 2 and Supplementary Figure 1) except within the substrate-binding (between the helices H4 and H5) and the HVR (see below) regions. Figure 2 provides a selected subset of the sequence alignments and the entire alignments of VAP1 and 39 ADAM sequences, including all 23 human ADAMs so far available, can be found as Supplementary Figure 1.

M-domain

Each VAP1 M-domain corresponds to a very similar structure to that of ADAM33 (Orth *et al*, 2004), with a flat ellipsoidal shape having a central core made up of five stranded β-sheets and five α-helices and a conserved methionine (Met-turn) below the active site histidine residues, which bears the typical structural feature of metzincin family of metalloproteinases (Bode *et al*, 1993). However, they differ in the dimer interface and the loop structure around the substrate-binding site (Figure 1C) that corresponds to the variable region in the primary structure (between the helices H4 and H5, see Figure 2). The N-terminal helix (H0) is also unique in VAP1. The dimer interface is best characterized by the recognition sequence QDHSK (residues 320–324, see Figure 1C and Supplementary Figure 2A–C) and by Cys365, however these are not conserved among ADAMs; therefore, none of the ADAMs' M-domains are suggested to form a stable dimer as VAP1. A peptide-like hydroxamate inhibitor GM6001 binds to VAP1 (Figure 1A and B, and Supplementary Figure 2D and E) in exactly the same manner as in the marimastat-ADAM33 M-domain complex (Orth *et al*, 2004), suggesting that the catalytic sites of VAP1 and ADAM33 share a common substrate recognition mechanism. The ADAM33